https://doi.org/10.5194/egusphere-2023-2677
Preprint. Discussion started: 16 November 2023

Comparison of the imaginary part of the atmospheric refractive index structure parameter and aerosol flux based on different measurement methods

Renmin Yuan[a] Hongsheng Zhang[b] Jiajia Hua[c] Hao Liu[d] Peizhe Wu[a] Xingyu Zhu[a] Jianning Sun[e]

[a] School of Earth and Space Science, University of Science and Technology of China, Hefei 230026, PR China
[b] Laboratory for Climate and Ocean-Atmosphere Studies, Department of Atmospheric and Oceanic Sciences, School of Physics, Peking University, Beijing 100081, PR China
[c] China Meteorological Administration Xiong'an Atmospheric Boundary Layer Key Laboratory, Xiong'an New Area 071800, PR China
[d] School of Mathematics and Physics Anhui Jianzhu University, Hefei 230601,PR China
[e] School of Atmospheric Sciences, Nanjing University, Jiangsu, 210093, PR China

Correspondence: Yuan Renmin (rmyuan@ustc.edu.cn)

Abstract: The complexity of aerosol particle properties and the diversity of characterizations make aerosol vertical transport flux measurements and analysis difficult. Although there are different methods, such as aerosol particle number concentration flux and aerosol mass flux based on the eddy covariance principle, and aerosol mass flux measurements based on the light-propagated large-aperture scintillation principle, there is a lack of mutual validation among the different methods. In this paper, a comparison of aerosol mass flux measurements based on the eddy covariance principle and aerosol mass flux measurements based on the light-propagated large aperture scintillation principle is carried out. The key idea of aerosol mass flux measurements based on the light-propagated large-aperture scintillation principle is the determination of the imaginary part of the atmospheric equivalent refractive index structure parameter (AERISP). In this paper, we will first compare the AERISPs measured by two different methods and then compare the aerosol mass vertical transport fluxes obtained by different methods. The experiments were conducted on the campus of the University of Science and Technology of China (USTC). The light propagation experiment was carried out between two tall buildings to obtain the imaginary and real parts of AERISPs for the whole path, which in turn can be used to obtain the aerosol vertical transport flux. An updated visibility meter is installed on the meteorological tower in the middle of the light path, which is utilized to obtain the single-point visibility, which is then converted to the imaginary part of the atmospheric equivalent refractive index (AERI). The imaginary parts of the AERISP were obtained using spectral analysis with visibility data. The results show that the imaginary parts of the AERISPs obtained by different methods are in good agreement. The imaginary part of the AERI measured by the visibility meter and the vertical wind speed obtained by the ultrasonic anemometer were used for covariance calculation to obtain the aerosol vertical transport flux. The trends of aerosol vertical transport fluxes obtained by different methods are consistent, and there are differences in some details, which may be caused by the inhomogeneity of the vertical transport of aerosol fluxes. The experimental results also show that urban green land is a sink area for aerosol particles.

Keywords: light propagation, scintillation, atmospheric equivalent refractive index, structure parameter, eddy covariance, aerosol fluxes

https://doi.org/10.5194/egusphere-2023-2677
Preprint. Discussion started: 16 November 2023

1 Introduction

Atmospheric aerosols are solid or liquid particles suspended in the atmosphere that can affect public health, reduce near-surface visibility, decrease direct radiation from the air, and act as condensation nuclei affecting cloud structure and distribution(McNeill, 2017;Rosenfeld et al., 2014). Human activities have dramatically altered air quality, climate and the Earth system. The expansion of urban, agricultural and industrial areas and changes in the nature of land use have increased aerosol concentrations. Due to the complexity of aerosols, many observations have been carried out from different perspectives. However, most of the current observations only measure the state characteristics of aerosols, such as concentration, particle size distribution, and composition, and what is obtained is an average characterization of aerosol properties(Krieger et al., 2012).

Aerosol particles in the atmosphere will follow atmospheric motion, which is manifested in the uneven distribution of aerosol particle concentrations in space and time. On the one hand, the unevenly distributed aerosol particles will have a corresponding effect on the light wave propagating in the atmosphere, and on the other hand, we can understand the distribution characteristics of aerosol particles based on the optical effect of aerosol particles and then obtain more information about the transportation of aerosols.

Previously, Yuan et al. (2015) introduced the concepts of the atmospheric equivalent refractive index (AERI) and the atmospheric equivalent refractive index structure parameter (AERISP). The AERI includes real and imaginary parts, and accordingly, the AERISP also includes real and imaginary parts of the structure parameters. When the working wavelength is in the atmospheric transparent band, the light wave is almost not absorbed by the gas components in the atmosphere, and the attenuation of the light wave is mainly caused by the extinction of aerosol particles. Theoretical analysis shows that the imaginary part of the AERISP is determined by the fluctuation of aerosol concentration. The real part of the AERISP corresponds to the atmospheric temperature variation. Furthermore, it is assumed that the aerosol concentration variations follow the same pattern as the scalar motion, which is in line with the similar theory of the surface layer, and thus, the vertical transport flux of aerosol particles in the near-surface layer can be obtained by using the imaginary part of the AERISP (Yuan et al., 2016;Yuan et al., 2019). AERISP observations are carried out in many places, and then the aerosol flux is obtained by combining the similarity theory. However, there is a lack of experimental verification of the imaginary structure parameter and aerosol flux observations. Currently, the imaginary part of the AERISPs is only obtained using large-aperture scintillometer (LAS) measurements, so it is necessary to carry out measurements of the imaginary part of the AERISPs based on other different methods, as well as measurements of aerosol fluxes based on different methods.

https://doi.org/10.5194/egusphere-2023-2677
Preprint. Discussion started: 16 November 2023

The reference to the measurement of the imaginary part of the AERISP and the aerosol vertical transport flux using the light propagation principle is naturally associated with the current widespread use of LASs based on the light propagation principle for the measurement of the sensible heat flux in the surface layer(Moene et al., 2009). Comparative validation of this measurement is obtained using eddy covariance (EC) techniques(Zhang and Zhang, 2015). EC measurements require a fast response of the sensing elements for wind speed and air temperature. Similar to the validation of LAS measurements of sensible heat fluxes, EC measurements were also considered for aerosol vertical transport flux validation. Measurements of aerosol particle number concentration fluxes using eddy covariance methods have been implemented at many locations(Gordon et al., 2011;Vogt et al., 2011;Ripamonti et al., 2013). We attempted to measure the aerosol particle number concentration flux using an eddy covariance system consisting of a fast-response particle counter with an ultrasonic anemometer, which has a response frequency of up to 10 Hz, and simultaneously measured parameters such as aerosol particle size distribution, mass concentration, forward scattering coefficient, and extinction coefficient to calculate the aerosol mass concentration flux. For half of the experimental period, the trend of the measurements with the two methods was the same, while the other periods differed greatly (experimental results unpublished). The reason may be the very weak extinction of aerosol particles with scales much smaller than the working wavelength.

According to the definition of the imaginary part of the AERISP, the validation work can be realized by choosing an instrument for rapid measurement of the atmospheric extinction coefficient and an ultrasonic anemometer to form an EC system. However, the direct and rapid measurement of the atmospheric extinction coefficient is difficult to realize. The imaginary part of the AERI is proportional to the atmospheric extinction coefficient and inversely proportional to the atmospheric visibility, so it is possible to analyze the results of the visibility meter to obtain the imaginary part of the AERISP at a certain point. However, the conventional visibility meter has a slow response and low sampling frequency, which is not suitable for correlating with the vertical velocity to obtain the aerosol flux, and Ren et al. (2020) improved the conventional visibility meter by obtaining visibility data at 1 Hz and then using the eddy covariance method to obtain the vertical aerosol transport flux based on the relationship between visibility and aerosol mass concentration(Ren et al., 2020). Inspired by their work, we use the improved visibility meter in this study to obtain visibility data at a higher frequency of 1 Hz and correlate the data with ultrasonic anemometer measurements to potentially utilize the obtained aerosol vertical transport fluxes to achieve experimental validation of the imaginary part of the AERISP and aerosol flux observations.

The theoretical and experimental introduction is given in the second part of the paper, the experimental results are given in the third part, and the conclusions and discussion are given in the fourth part.

https://doi.org/10.5194/egusphere-2023-2677
Preprint. Discussion started: 16 November 2023

2 Theoretical methods and experiments

The AERISP and the aerosol vertical transport flux are the topics of interest in this paper. In this section, definitions and theoretical expressions for these parameters are given, as well as how the measurements were carried out.

2.1 The imaginary part of the AERISP

When the beam is transmitted in the atmosphere, in addition to the unevenly spatial distribution of the beam energy due to the refraction diffraction phenomenon caused by the fluctuation of the refractive index caused by the fluctuation of temperature, the beam energy is also attenuated by the absorption and scattering of aerosol particles. Therefore, the atmosphere and aerosol particles can be taken as a whole, called the equivalent medium; thus, the equivalent refractive index n_{equ} concept is introduced (van de Hulst, 1957;Yuan et al., 2021),

$$n_{equ} = n_m + i\frac{2\pi}{\eta^3}\int_0^\infty S(0)\frac{dN}{dD}dD \quad (1)$$

where n_m is the refractive index of atmospheric molecules, η is the wavenumber of light waves, and i denotes an imaginary number. S(0) is the forward scattering function (0 in parentheses is the scattering angle). N is the number of aerosol particles per unit volume, and dN/dD is the size distribution of aerosol particle sizes.

The equivalent refractive index consists of real and imaginary parts denoted by n_{Re} and n_{Im}, respectively, i.e., $n_{eff} = n_{Re} + in_{Im}$. The real part is the refractive index of the molecule, and the imaginary part is.

$$n_{\mathrm{Im}} = \frac{2\pi}{\eta^3}\int_0^\infty \mathrm{Re}[S(0)]\frac{dN}{dD}dD \quad (2)$$

It is known that the atmospheric extinction coefficient has a similar form(Liou, 2002):

$$\beta_{ext} = \frac{4\pi}{\eta^2}\int_0^\infty \mathrm{Re}[S(0)]\frac{dN}{dD}dD \quad (3)$$

From Eqs (2) and (3), we can see that

$$n_{Im} = \lambda\beta_{ext}/4\pi \quad (4)$$

where λ is the working wavelength (λ=2π/η). Based on the relationship between the aerosol extinction coefficient and visibility (V) (V=3.912/β_{ext}), the aerosol extinction coefficient can be deduced from visibility measurements, and then the imaginary part of the AERI can be obtained based on Eq. (4).

Experiments show that the temperature fluctuation satisfies the turbulence "2/3" law(Liu et al., 2017), and according to the relationship between temperature and the real part of the AERI, the fluctuation of the real part of the AERI also satisfies the turbulence "2/3" law; thus, we can define the structure parameter of temperature, C_T^2, and the real part of the AERISP $C_{n,Re}^2$. Therefore, general scalars can be extended, such as the fluctuation of the imaginary part of the AERISP and the

https://doi.org/10.5194/egusphere-2023-2677
Preprint. Discussion started: 16 November 2023

fluctuation of the atmospheric extinction coefficient. Thus, we can assume that the imaginary part of the AERI satisfies the turbulence "2/3" law.

$$D_{n,\mathrm{Im}}(r) = \overline{[n_{\mathrm{Im}}(\vec{x}) - n_{\mathrm{Im}}(\vec{x}+\vec{r})]^2} = C_{n,\mathrm{Im}}^2 r^{2/3} \tag{5}$$

Thus, we can introduce the imaginary part of AERISP $C_{n,Im}^2$, a parameter used to describe the fluctuation intensity of the imaginary part of the AERI. Correspondingly, we can introduce the structure parameter of the atmospheric extinction coefficient $C_{\beta_{ext}}^2$ and the structure parameter of the fluctuation of the aerosol mass concentration C_M^2.

2.2 Two methods of equivalent refractive index structure parameter measurement

From the definition of the AERISP in the last part and the relationship between the AERI and the extinction coefficient, it can be seen that the AERISP has an important influence on light propagation in the atmosphere, and thus the AERISP can be estimated from the light intensity fluctuation in light propagation and the monitoring of the extinction coefficient. The section describes how to measure the AERISP with the help of two methods.

2.2.1 Long-Path Light Propagation Methods

When an approximately collimated light beam in the transparent band of the atmosphere is selected and propagated over a distance, the light intensity at the receiving end fluctuates. The fluctuation in light intensity has two causes: one is the uneven distribution of the real part of the AERI caused by the temperature fluctuation, and the other is the uneven distribution of the imaginary part of the AERI caused by the uneven distribution of aerosol particles. Assuming that the above two causes are not related, they can be decomposed. Theoretical analysis shows that the power spectral density expression for the part of the contribution of the inhomogeneous distribution of the imaginary part of the AERI to the fluctuation of the light intensity is(Yuan et al., 2015).

$$W_{\ln I,\mathrm{Im}}(f) = 64\pi^2\eta^2 \int_0^L dx \int_{2\pi f/v}^{\infty} \Phi_{n,\mathrm{Im}}(\kappa)\cos^2\left[\frac{\kappa^2 x(L-x)}{2\eta L}\right]\left[(\kappa v)^2 - (2\pi f)^2\right]^{-1/2} \cdot \left[\frac{2J_1\left(\frac{D_r\kappa x}{2L}\right)}{D_r\kappa x/2L}\right]^2 \left[\frac{2J_1\left(\frac{D_t\kappa(L-x)}{2L}\right)}{D_t\kappa(L-x)/2L}\right]^2 \kappa d\kappa \tag{6}$$

where f is the frequency of the log-intensity spectrum, η is the wavenumber of the spherical wave (η=2π/λ, λ is light wavelength), x is the position of the propagating wave, L is the length of the propagation path, κ is the wavenumber of the two-dimensional log-intensity spectrum, and $\Phi_{n,Im}$ is the spectrum of the imaginary parts of the refractive index, where the subscript n denotes the refractive index and the subscript Im denotes the imaginary parts of the refractive index. The widely used von Karman spectral form for $\Phi_{n,Im}$ is adopted in this study (Andrews and Phillips, 2005), which can be expressed as follows:

https://doi.org/10.5194/egusphere-2023-2677
Preprint. Discussion started: 16 November 2023

$$\Phi_{n,\mathrm{Im}}(\kappa)=0.033C_{n,\mathrm{Im}}^{2}(\kappa^{2}+\frac{1}{L_{0}^{2}})^{-\frac{11}{6}}e^{-\frac{\kappa^{2}l_{0}^{2}}{5.92^{2}}} \tag{7}$$

Here, L_0 is the outer scale of turbulence, and l_0 is the inner scale of turbulence.

Substituting Eq. (7) into Eq. (6) and integrating the right-hand side of Eq. (6) yields,

$$W_{\ln I,\mathrm{Im}}(f)=0.129C_{n,\mathrm{Im}}^{2}\eta^{2}Lv^{5/3}[f^{2}+(\frac{v}{2\pi L_{0}})^{2}]^{-4/3} \tag{8}$$

Using Eq. (8), the imaginary part of the AERISP can be determined based on the shape of the spectrum while being constrained by the low-frequency variance of light intensity fluctuation from the imaginary part of AERISP.

To carry out a comparative analysis with the results of the real part of the AERISP, the expression for the power spectral density of the logarithmic light intensity fluctuation due to the real part of the AERI is also given here as (Clifford, 1971;Nieveen et al., 1998),

$$W_{\ln I,\mathrm{Re}}(f)=64\pi^{2}\eta^{2}\int_{0}^{L}dx\int_{2\pi f/v}^{\infty}\Phi_{n,\mathrm{Re}}(\kappa)\sin^{2}[\frac{\kappa^{2}x(L-x)}{2\eta L}][(\kappa v)^{2}-(2\pi f)^{2}]^{-1/2}\cdot$$

$$[\frac{2J_{1}(\frac{D_{r}\kappa x}{2L})}{D_{r}\kappa x/2L}]^{2}[\frac{2J_{1}(\frac{D_{t}\kappa(L-x)}{2L})}{D_{t}\kappa(L-x)/2L}]^{2}\kappa d\kappa \tag{9}$$

Integrating Eq. (9) yields the fluctuation variance of the log light intensity as

$$\sigma_{\ln I,\mathrm{Re}}^{2}=\int_{0}^{\infty}W_{\ln I,\mathrm{Re}}(f)df=0.89C_{n,\mathrm{Re}}^{2}L^{3}D_{t}^{-7/6}D_{r}^{-7/6} \tag{10}$$

The real part of AERISP is usually calculated using Equ. (10) (Wang et al., 1978).

2.2.2 Spectral analysis methods for single-point measurements

Aerosol particles follow atmospheric motion, which is consistent with general atmospheric motion characteristics, and the "-5/3" law can be used to characterize the fluctuations in aerosol-related properties. Therefore, in the inertial subregion, the extinction coefficient power spectral density is

$$S_{\beta_{ext}}(f)=(2\pi/U)S_{\beta_{ext}}(\kappa)=0.25C_{\beta_{ext}}^{2}(2\pi/U)^{-2/3}f^{-5/3} \tag{11}$$

The extinction coefficient structure parameter $C_{\beta_{ext}}^2$ can be converted to the imaginary part of the AERISP according to equation (4). The coefficient in Eq. (11) is 0.25(Wyngaard et al., 1971). It has been suggested in the literature that the coefficient for the spectral density should be 0.125(Gibbs and Fedorovich, 2020). The difference between the two coefficients 0.25 and 0.125 is whether the integral of the spectral density is equal to the variance or half of the variance. If the integral of the spectral density is equal to the variance, the coefficient of 0.25 is taken; if the integral of the spectral density is equal to half of the variance, the coefficient is taken as 0.125. According to the spectral density curve, the coefficients are determined within the inertial subregion, and then the structure

https://doi.org/10.5194/egusphere-2023-2677
Preprint. Discussion started: 16 November 2023

parameters $C^2_{\beta_{ext}}$ can be obtained. According to the relationship between the extinction coefficient and the imaginary part of the AERI in Eq. (4), the imaginary part of the AERISP can be obtained as $C^2_{n,Im}$.

Similarly, power spectral density profiles with temperature fluctuations that

$$S_T(f) = (2\pi / U) S_T(\kappa) = 0.25 C_T^2 (2\pi / U)^{-2/3} f^{-5/3} \tag{12}$$

The actual temperature turbulence spectral density profile often takes the form of a von Karman spectrum as

$$S_T(f) = 0.25 C_T^2 (2\pi / U)^{-2/3} \left(f^2 + (\frac{U}{2\pi L_0})^2 \right)^{-5/6} \tag{12'}$$

Based on the relationship between temperature and the real part of the AERI, we have

$$C_n^2 = C_T^2 / R_{TN}^2 \tag{13}$$

where R_{TN} denotes the coefficient of proportionality between the change in the real part of the AERI and the change in atmospheric temperature.

$$R_{TN} = \frac{dT}{dn_{\mathrm{Re}}} = -1.29 \times 10^4 \times (1 + \frac{7.52 \times 10^{-3}}{\lambda^2})^{-1} \frac{\overline{T}^2}{\overline{P}} \tag{14}$$

where the wavelength λ is in microns, the atmospheric pressure P is in hectopascals, and the temperature T is in kelvin.

The real part of the AERISP can be obtained by fitting the experimental data using Eqs. (12) or (12').

2.3 Flux estimation

The method for estimating the AERISP was given in the former sections. The purpose of estimating the AERISP in this paper is to estimate the aerosol flux in the near-surface layer. Here, the method of estimating the aerosol flux based on the AERISP will be given first, and then the method of estimating the aerosol vertical transport flux based on the EC technique will be introduced.

2.3.1 Optical transmission method

Experiments have shown that the AERISPs satisfy the theory of surface layer similarity; thus, (Yuan et al., 2019)

$$F_{a\_LAS} = (\frac{C^2_{n,\mathrm{Im}}}{C^2_{n,\mathrm{Re}}})^{1/2} \frac{R_{MN}}{R_{TN}} u_* |T_*| \tag{15}$$

where u_* is the friction velocity and T_* is the characteristic potential temperature. These two parameters can be determined from wind speed and temperature profiles. The real and imaginary parts of the AERISP are determined from LAS measurements. R_{MN} can be obtained from aerosol mass concentration and visibility measurements (R_{MN} = M/n_{Im}, where M is the aerosol mass concentration approximated as PM_{10} and n_{Im} can be determined from visibility measurements)(Yuan

https://doi.org/10.5194/egusphere-2023-2677
Preprint. Discussion started: 16 November 2023

et al., 2021), and R_{TN} can be calculated from mean air temperature and other measurements using Eq. (14) again.

When turbulence of the surface layer is developed, Eq. (15) can be approximated as(Yuan et al., 2019),

$$F_{a\_LAS} = a(\frac{g}{T})^{1/2} R_{TN}^{1/2} (C_{n,\mathrm{Re}}^2)^{1/4} R_{MN} (C_{n,\mathrm{Im}}^2)^{1/2} (z-d) \tag{16}$$

Here, a is the scale factor with a theoretical value of 0.567 (which needs to be determined by comparative experiments), g is the gravitational acceleration, z is the scintillator height, and d is the zero-plane displacement. Equation (16) does not require measurement of u_* and T_* data. Generally, the measurement heights are high, and the assumption of developed turbulence in the surface layer is easily met during the day under unstable conditions.

2.3.2 Based on single-point eddy covariance

Eddy covariance is a commonly used method for the measurement of Earth air exchange fluxes in the near-surface layer. Using rapid measurements of vertical wind speed and extinction coefficient to obtain the ups and downs of the vertical wind speed and extinction coefficient, the expression for the vertically transported aerosol flux calculated by the eddy-covariance method with the mean vertical velocity close to zero is given by(Wilczak et al., 2001)

$$F_{a\_EC} = R_{MN} \frac{\lambda}{4\pi} \overline{w' \beta_{ext}'} \tag{17}$$

The prime' in Eq. (17) denotes fluctuation.

2.4 Introduction to the experiment

The experiments were performed on the campus of the University of Science and Technology of China (USTC) in Hefei, Anhui Province, China. The campus of the University of Science and Technology of China (USTC) is located in downtown Hefei. Figure 1a gives part of the Hefei city area, where the red rectangle corresponds to Fig. 1b, the campus of USTC. The campus is surrounded by four highways, and the two highways in the west and north have more vehicles, especially the viaduct in the west. The campus is composed of vegetation, roads and teaching buildings. As can be seen in Fig. 1b, green vegetation covers most of the campus. The roofs of the school buildings are almost on a plane with the tree canopy and are approximately 17 meters above the ground. The zero plane displacement in Eq.(16) is taken 17 meters. There are two tall buildings (T and R in Fig. 1b) at the southernmost and northernmost parts of the campus, and the distance between the two buildings is approximately 960 meters. The experiment consists of two parts: one part is to carry out the light propagation experiment using a self-developed large aperture scintillator (LAS), and the other part is to carry out the measurement using the instruments on the meteorological tower in the middle of the beam. The transmitting end of the LAS was installed on the 12th floor of the southernmost building (T in Fig. 1b), the receiving end was installed on the 12th floor of the northernmost building (R in Fig. 1b), and the distance of the beam from the ground was approximately 35 meters. The apertures of the transmitting and receiving ends were 250 mm. The sampling frequency of the receiving end was 500 Hz, and a data file was saved every 30 minutes. The height of the meteorological tower is 18 meters above the roof of a teaching building (P in Fig.

https://doi.org/10.5194/egusphere-2023-2677
Preprint. Discussion started: 16 November 2023

1b). The top of the meteorological tower is equal to the height of the beam. The meteorological tower is equipped with 5 layers of wind speed and direction temperature and humidity measurement sensors. At the top of the tower, there is a radiation quadrature sensor, and at the bottom of the tower, there is a rainfall measurement sensor. In this paper, we use data from the top 18-meter height position of the meteorological tower with sensors installed for conventional meteorological parameters, including temperature, humidity, wind speed, and wind direction radiation. Conventional meteorological data are collected at 1-second intervals, average data are obtained every half hour after data collection, and precipitation data are recorded every half hour. A three-dimensional sonic anemometer thermometer was installed at the top of the tower, and a high-frequency sampling visibility sensor CS120A (Campbell, 2012) was upgraded to have the ability to obtain a 1-Hz visibility (Ren et al. 2020). The three-dimensional sonic anemometer thermometer can obtain a sampling frequency of over 10 Hz and is a common instrument used in atmospheric turbulence research; as such, we will not introduce it in depth. To correlate the vertical wind speed with the extinction coefficient to obtain the aerosol flux, the data collected by the sonic anemometer-thermometer at 10 Hz were averaged to obtain 1-Hz data, which were saved in a data file.

The time period of the experiment is January 9-23, 2022, a total of 15 days.

2.5 Data quality control

Data obtained from field observations need to be controlled for data quality before further processing (Foken and Wichura, 1996). This study involves several types of data, mean variables, cumulative variables, and fluctuating variables. Mean variables include 30-minute averages of temperature, humidity, wind speed, wind direction, and global radiation. Data quality control for mean variables was performed by comparing measurements at different heights or different sites. The same variables with the same trend at different heights and different locations were considered to be high quality data. All measured mean data were determined to be satisfactory. Cumulative variables refer to 30-minute rainfall data. Rainfall data were qualified with reference to relative humidity, total radiation and air temperature. Fluctuating data included 10-Hz ultrasonic anemometer data and 1-Hz visibility data, as well as high-frequency intensity fluctuation data measured by the LAS, the real and imaginary parts of the AERISP, and calculated aerosol fluxes. Quality control consisted mainly of eliminating spikes and replacing missing data.

The reason for the spike points in the light intensity fluctuation data is that the received signal jumps when there are flying birds and other obstructions to the optical signal on the propagation path. This situation is automatically determined by the program. When this occurs, the data for that time period will not be processed. The AERISP and aerosol flux data are judged according to (a) three times the standard deviation (SD) from the mean value and (b) three times the standard deviation from the mean of differences between adjacent moment data. To determine the three times standard deviation from the mean value, the trend is obtained by averaging over a two-hour period, then calculating the difference between the measured value and the trend at each moment, calculating the mean and variance of the difference, and considering a spike point if the difference is outside the 3 times standard deviation. The 3 times standard deviation of adjacent differences is determined by first calculating the difference between adjacent moments and then calculating the mean and standard deviation of the difference. Any data that deviates from the mean by more than 3 times the standard deviation is considered a spike point.

https://doi.org/10.5194/egusphere-2023-2677
Preprint. Discussion started: 16 November 2023

Data judged to be a spike will be supplemented by the average of adjacent moments. Of course, data processed according to this method appear to be completely missing for longer time periods. For such cases, no further methods to realize supplementation are considered in this paper. There are other errors in measurements made with the LAS that are due to specific reasons (Moene et al., 2009); for example, the effect of spectral shape deviations using the von Karman model and intermittent variations in the properties of this spectrum on the LAS signal is not considered in this study.

Similar to CO_2 flux calculation, EC calculations for aerosol flux were performed to obtain aerosol fluxes, and several data quality control work was conducted, such as coordinate system rotations(Wilczak et al., 2001;Yuan et al., 2011), WPL corrections(Webb et al., 1980).

3 Experimental results

In the following, the variation curves of conventional meteorological parameters during the experimental period, individual examples of AERISPs, a comparison of the two methods for the results of multiday continuous observations and a comparison of the two methods for the results of flux measurements will be presented to verify the reliability of the means of light propagation measurement.

3.1 General meteorological parameters and extinction coefficients

The variation curves of conventional meteorological parameters during the experiment, including temperature, humidity, wind speed, wind direction, radiation and precipitation, and extinction coefficient are shown in Fig. 2, where the extinction coefficient is calculated from the visibility ($\beta_{ext} = 3.912/V$, V denotes visibility). Seven days during the experiment were sunny, and four of the remaining eight days had rainfall. The temperatures on sunny days were characterized by significant daily variations, with a minimum temperature of 0.4°C, and the maximum diurnal temperature difference could reach more than 9°C. Relative humidity exceeded 80% for only a few periods during the sunny days. The wind speed was generally less than 3 m/s, and there were only very few periods of north wind with a speed of more than 3 m/s. There was no obvious prevailing wind direction during the experimental period, and only the north wind was equivalent to the other directions with a slight predominance. The meteorological conditions during the experiment were similar to those of the local winter season. The extinction coefficient curve with time during the experiment is given in Fig. 2(g). The pollution gradually increased from the 9th to Jan. 13th and decreased on the 13th; from the 14th to the 20th, the pollution gradually increased and decreased on the 20th. The meteorological conditions during the experimental period can be considered typical.

3.2 Example results from measurements of the imaginary part of the AERISP

Before carrying out the comparison of the measurement results of the two methods for obtaining the AERISP, the comparison of the measurement results of an individual example is given. The experimental data measured from 2022-01-16 13:00-13:30 will be used here as an example to illustrate the calculation of the AERISP, and the results will be given. This time period is midday on

https://doi.org/10.5194/egusphere-2023-2677
Preprint. Discussion started: 16 November 2023

a clear day (shown in Fig. 2e), and both the total radiation and sensible heat fluxes are large, so this time period can be taken as a good typical example.

3.2.1 Structure parameters obtained by light propagation

The AERISP is first given using the light propagation method. The sequence of light intensity signals obtained at the receiving end is shown in Fig. 3a. The time duration is 2022-01-16 13:00-13:30, and the sampling frequency is 500 Hz, so there are 900000 data points in the time series of light intensity fluctuation in Fig. 3a. The curve has both low- and high-frequency fluctuations. Using spectral analysis and correlation analysis, the variance of the low-frequency part of the logarithmic light intensity is 1.08e-4, and the variance of the high-frequency part is 5.06e-4. The solid dots in Fig. 3b are the measured spectral densities of the logarithmic light intensity fluctuations, and the black dashed lines and solid lines represent the results calculated by Eqs. (6) and (9), respectively, and represent the contributions of the imaginary part and the real part. As seen from the power spectral density curves of the logarithmic light intensity fluctuations in Fig. 3b, the high-frequency part and the low-frequency part have different characteristics.

In the logarithmic plot, the low-frequency part is prominent with a much higher spectral density than the high-frequency part. Theoretical analysis shows that the low-frequency part corresponds to the contribution of the imaginary part of the AERISP. The high-frequency part is flat plus high-frequency attenuation. The high-frequency part corresponds to the contribution of the real part. The part greater than 100 Hz is noise.

Based on the previous theoretical approach, the spectral density fitting for the low-frequency part, while constrained by the low-frequency variance, yields an equivalent refractive index structure parameter of $1.14 \times 10^{-25} m^{-2/3}$. Correspondingly, the structure parameter of the real part of the refractive index, based on the high-frequency variance, is obtained as $2.54 \times 10^{-14} m^{-2/3}$.

3.2.2 Obtaining the imaginary part of the AERISP based on the spectrum

The coefficients of the power spectral density curves are proportional to the refractive index structure parameters, from which they can be determined. The extinction coefficient structure parameter can be deduced from the power spectral density of the extinction coefficient fluctuation, and the temperature structure parameter can be deduced from the power spectral density of the temperature fluctuation. The extinction coefficient (Fig. 4a) and temperature (Fig. 4b) fluctuation with time for the period 2022-01-16 13:00-13:30 are given in Fig. 4. As shown in Fig. 4, the extinction coefficient curve has more noise, while the temperature curve has less noise. On the temperature fluctuation curve, there are five distinct ramp structures.

Power spectral analysis of the data in Fig. 4 was carried out to obtain the power spectral density in Fig. 5. From the extinction coefficient power spectral density curve in Fig. 5a, it can be seen that spectral densities greater than 0.05 Hz exhibit noise, and spectral densities less than 0.05 Hz have inertial subregions. When practically analyzed, the inertial subregion ranges from 0.002 Hz to the noise onset frequency. The motion of aerosol particles in the atmosphere conforms to the "-5/3" law of turbulence. The extinction coefficient structure parameter was obtained by fitting the data in the

https://doi.org/10.5194/egusphere-2023-2677
Preprint. Discussion started: 16 November 2023

inertial subregion using Eq. (11) with a value of $3.9 \times 10^{-11}\mathrm{m}^{-2}m^{-2/3}$, which was then converted to the structure parameter of the imaginary part of the refractive index of $1.04 \times 10^{-25}m^{-2/3}$.

Correspondingly, as seen from the temperature fluctuation power spectrum curve in Fig. 5b, almost no noise appears, which is mainly due to the small noise of the temperature signal itself, while the 1 Hz temperature data here are obtained by averaging the data collected at 10 Hz. The temperature structure parameter of 0.0218°C^2 $\mathrm{m}^{-2/3}$ is obtained by fitting using Eq. (12), which is converted to a refractive index real part structure parameter of $2.1 \times 10^{-14}m^{-2/3}$.

The imaginary part of the AERISP obtained by using a visibility meter and the real part of the AERISP obtained by an ultrasonic anemometer are in good agreement with the previous results given by using optical propagation means.

3.3 Comparison of all results for the AERISP

The previous section gives an individual example. A comparison of all the data during the experiment is given below, as shown in Figs 6 and 7.

A comparison of the time series of AERISPs measured by the two methods is given in Fig. 6, where Fig. 6a shows the time series of the imaginary part of the AERISP and Fig. 6b shows the time series of the real part of the AERISP. It can be seen that there are large fluctuations in the imaginary part of the AERISP during the experimental period. This trend is close to that of the aerosol extinction coefficient. From Fig. 6a, it can be seen that there is no obvious daily variation characteristic. The trend agreement of the results obtained by the two methods is very good. From Fig. 6b, it can be seen that the real part of the AERISP on sunny days has obvious daily variation characteristics, which are large during the day and small at night. The agreement of the results obtained by the two methods is good during the daytime, and at night, the results obtained by the light propagation method are larger than those of the large point measurements.

Scatter plots of the results of the measurements of the two methods are given in Fig. 7. Figure 7a shows the scatter plot of the results of the two methods for the imaginary part of the AERISP with a correlation coefficient R^2 of 0.73, while Fig. 7a shows the scatter plot of the results of the two methods for the real part of the AERISP with a correlation coefficient of real R^2 of 0.62. This shows that the correlation coefficients of the imaginary structure parameters obtained by the two methods are larger than those of the real structure parameters. The reason for the smaller correlation coefficient of the real part of the AERISP is that the difference in the real part of the AERISP obtained by the two methods at night is larger. This shows that the aerosol spatial distribution at night may be more homogeneous than the temperature distribution. The reason for this may be that the temperature distribution in the overlying surface of the campus at night is not uniform, and weak turbulence does not produce strong mixing, resulting in a non-uniform distribution of the real part of the AERISP. There are no strong aerosol emission sources on the nighttime campus, so the distribution of the imaginary part of the AERISP behaves more uniformly.

3.4 Velocity-extinction coefficient correlation for a single point

To calculate aerosol fluxes using EC techniques, delayed correlation of vertical velocity and extinction coefficient is needed. The delayed correlation curves of the vertical velocity and extinction coefficient is given in Fig. 8.

https://doi.org/10.5194/egusphere-2023-2677
Preprint. Discussion started: 16 November 2023

The horizontal coordinate of the delay correlation curve in Fig. 8 is the delay time τ and the vertical coordinate is the delay correlation. From Fig. 8, it can be seen that at τ = -2 s, the correlation curve has an obvious extreme value, which is also the minimum value of the delay time in duration of 300 s. The minimum value is -5.22e-6m^{-1}. The reason that the extreme value of the correlation curve does not appear at 0 s is that there is a distance of about 0.20 m between the sensing element of the visibility meter and that of the ultrasonic anemometer. Here are given the cases with obvious extremes, and there are some cases where no obvious extremes appear. In such cases where there are no significant extremes, the value associated with a delay time of 0 seconds is taken.

3.5 Flux

The AERISP was given in the former part, and the aerosol vertical transport flux can be estimated for the duration of 2022-01-16 13:00-13:30 according to Eq. (16),

$$F_{a\_LAS} = 0.567 * \left(\frac{9.8}{283}\right)^{\frac{1}{2}} * (1.01 \times 10^6)^{\frac{1}{2}} * (2.54 \times 10^{-14})^{\frac{1}{4}} * 6216 * (1.14 \times 10^{-25})^{1/2} * 18 * 10^9 = 1.60\ \mu\text{gm}^{-2}\ \text{s}^{-1} \tag{18}$$

Where a=0.567, T=283K, g=9,.8m/s^2, $R_{TN} = 1.01 \times 10^6 K$, $C_{n,Re}^2 = 2.54 \times 10^{-14} m^{-2/3}$, $R_{MN} = 6216 Kg \cdot m^{-3}$ (Yuan et al., 2015), $C_{n,Im}^2 = 1.14 \times 10^{-25} m^{-2/3}$, z=35m, d=17m.

Similarly, the aerosol flux is obtained from the eddy covariance method according to Eq.(17)

$$F_{a\_EC} = -0.522 \times 10^{-6} * 6216 * 10^9 * \frac{0.65 \times 10^{-6}}{4\pi} = -1.67\ \mu\text{gm}^{-2}\ \text{s}^{-1} \tag{19}$$

Where $\overline{w'\beta_{ext}'} = -0.522 \times 10^{-6} s^{-1}$, $R_{MN} = 6216 Kg \cdot m^{-3}$, $\lambda = 0.65 \times 10^{-6} m$.

From the previous calculations, we can see that during the half hour 2022-01-16 13:00-13:30, the absolute values of the aerosol fluxes obtained by the two methods are very close, but of opposite sign. Since the LAS method based on light propagation cannot determine the direction of flux transport, only the magnitude of the flux can be given. This is similar to the fact that the estimation of surface sensible heat fluxes using a LAS also gives only the magnitude but not the direction. There are some judgments for estimating the direction of sensible heat flux using a LAS, such as those based on sunrise and sunset times and atmospheric stability (Zhao et al., 2018). Here, the flux is negative to indicate the deposition of aerosol particles. Because the experimental site is a campus, there is almost no source of aerosol particle emission in the overlying surface, which is manifested as a sink of aerosol particles inside the city. Therefore, the direction of aerosol flux measurement based on the LAS needs to be judged based on the nature of the subsurface.

The results of aerosol flux calculations throughout the experiment, except two days of rain, the 22nd and 23rd. are given in Fig. 9. Figure 9a shows the absolute values of the aerosol vertical transport fluxes measured by the two methods based on the imaginary part of the AERISP and EC methods, and Fig. 9b shows the aerosol vertical transport fluxes with sign for transport direction measured, which correspond to the rectangle-point line in Fig. 9a. The trend of aerosol fluxes obtained by the two methods given in Fig. 9a is consistent with a diurnal variation in aerosol fluxes on sunny days, with larger values of aerosol fluxes at noon. At night, the aerosol flux values are smaller. Based on a comparison between Fig. 9a and Fig. 9b, it is shown that the aerosol flux is negative at noon on clear days, indicating that the turbulence is strong at noon, which enhances the downward transport of aerosol particles.

https://doi.org/10.5194/egusphere-2023-2677
Preprint. Discussion started: 16 November 2023

This study was conducted in a campus with no emission sources, and the downward flux is reasonable; in fact, there was an upward flux measured by the EC method if there were emission sources in the observation area (Ren et al. 2020).

4 Conclusion and discussion

To validate the previously developed method of measuring the AERISP and the aerosol mass flux, this paper theoretically organizes the concept of the AERISP, introduces two methods of measuring the AERISP and estimating the aerosol vertical transport flux by using the AERISP and EC methods, and carries out field observation experiments in an urban area. The experimental results show that the AERISPs estimated by the two methods are in good agreement, and the aerosol vertical transport fluxes obtained by the two methods based on the AERISP and EC are in good agreement.

According to the experimental results, the imaginary part of the AERISP expresses the intensity of the fluctuation of the attenuation of light during transmission. When the air-transparent band is used, the imaginary part of the AERISP characterizes the intensity of the fluctuation of the extinction coefficient of the aerosol.

The aerosol flux is related to both the fluctuations in aerosol concentration and the intensity of atmospheric turbulence. When there is an aerosol emission source on the overlying surface, the aerosol flux is positive, transporting aerosol particles upwards. When there is no aerosol emission source in the overlying surface, the overall performance is aerosol particle deposition and downwards transport of flux. In general, urban green lands are areas of aerosol particle deposition, while ocean and desert surfaces can often be viewed as source areas for aerosols.

From the experimental results, we can also see that, as a comparison, this paper also gives results for the temperature refractive index structure parameters, and as seen in Fig. 6, the trends for the structure parameters in the real and imaginary parts of the AERISP are different, indicating that temperature fluctuations and aerosol concentration fluctuations are uncorrelated. The purpose of this paper is to illustrate the physical significance of the structure constants of the imaginary part of the AERISP obtained using the LAS technique and to obtain the aerosol vertical transport flux based on the AERISPs. In inverting the imaginary part of the AERISP using the light propagation principle, there is an assumption that the aerosol concentration fluctuations are not correlated with the temperature fluctuations. This assumption cannot be proved theoretically. From the experimental results, as can be seen in Fig. 6, the trends of the real and imaginary parts of the AERISP are different, indicating that the temperature fluctuations and the aerosol concentration fluctuations are uncorrelated. This phenomenon shows that the two sources are different, which is basically consistent with the actual situation. This also shows that the assumptions of the theory for obtaining the imaginary part of the AERISP are reasonable.

In order to compare with aerosol transport fluxes obtained based on the AERISPs, this paper uses delayed correlation between the visibility meter and vertical wind speed to obtain aerosol vertical transport fluxes. Currently, a modified visibility meter is utilized to obtain 1 Hz visibility data, and then the extinction coefficient is obtained. From the extinction coefficient power spectrum in Fig. 5a, it can be seen that there is a large amount of noise in the high-frequency part. The signal-to-noise ratio of the extinction coefficient data is too low compared to the temperature fluctuation or velocity fluctuation, which introduces a large error in the calculation of the aerosol flux. Although the overall trend magnitude agreement of the fluxes obtained by the two methods is good enough to show that the two methods can be corroborated with each other, there are still differences in the details, which require technical methods to improve the performance of the instrument and to obtain high-quality aerosol extinction coefficient data in order to carry out the measurements of vertical aerosol transport fluxes based on EC method at a single point.

Data availability. Requests for data that support the findings of this study can be sent to rmyuan@ustc.edu.cn.

Competing interests. The authors declare that they have no conflict of interest.

Author contributions. Renmin Yuan and Hongsheng Zhang designed experiments and wrote the manuscript; Renmin Yuan, Jiajia Hua, Hao Liu, Xingyu Zhu and Peizhe Wu carried out experiments; Renmin Yuan analyzed experimental results. Jianning Sun revised the manuscript and participated in the discussion.

Acknowledgements. This study was supported by the National Natural Science Foundation of China (42075131) and the National Key Research and Development Program under grant no. 2022YFC3700701.

Reference

[1] Andrews, L. C., and Phillips, R. L.: Laser beam propagation through random media, SPIE, SPIE, Bellingham, Washington, USA, 2005.
[2] Campbell, S. L.: CS120 Visibility Sensor User Guide, Campbell Scientific Ltd., Logan, Utah 60 pp., 2012.
[3] Clifford, S. F.: Temporal-frequency spectra for a spherical wave propagating throught atmospheric turbulence, J. Opt. Soc. Am, 61, 1285-1292, 1971.
[4] Foken, T., and Wichura, B.: Tools for quality assessment of surface-based flux measurements, Agricultural and Forest Meteorology, 78, 83-105, 10.1016/0168-1923(95)02248-1, 1996.
[5] Gibbs, J. A., and Fedorovich, E.: On the Evaluation of the Proportionality Coefficient between the Turbulence Temperature Spectrum and Structure Parameter, Journal of the Atmospheric Sciences, 77, 2761-2763, 10.1175/jas-d-19-0344.1, 2020.
[6] Gordon, M., Staebler, R. M., Liggio, J., Vlasenko, A., Li, S.-M., and Hayden, K.: Aerosol flux measurements above a mixed forest at Borden, Ontario Atmos. Chem. Phys., 11, 6773-6786, 2011.
[7] Krieger, U. K., Marcolli, C., and Reid, J. P.: Exploring the complexity of aerosol particle properties and processes using single particle techniques, Chemical Society Reviews, 41, 6631-6662, 10.1039/c2cs35082c, 2012.
[8] Liou, K. N.: An Introduction to Atmospheric Radiation, 2nd Edition ed., Academic Press, California 92101-4495, USA, 2002.
[9] Liu, H., Yuan, R., Mei, J., Sun, J., Liu, Q., and Wang, Y.: Scale properties of anisotropic and isotropic turbulence in the urban surface layer, Boundary-Layer Meteorology, 165, 277-294, 2017.
[10] McNeill, V. F.: Atmospheric Aerosols: Clouds, Chemistry, and Climate, in: Annual Review of Chemical and Biomolecular Engineering, Vol 8, edited by: Prausnitz, J. M., Annual Review of Chemical and Biomolecular Engineering, 427-444, 2017.
[11] Moene, A. F., Beyrich, F., and Hartogensis, O. K.: Developments in scintillometry, Bulletin of the American Meteorological Society, 90, 694-698, 10.1175/2008bams2672.1, 2009.
[12] Nieveen, J. P., Green, A. E., and Kohsiek, W.: Using a large-aperture scintillometer to measure absorption and refractive index fluctuations, Bound-Lay. Meteorol., 87, 101-116, 1998.
[13] Ren, Y., Zhang, H., Wei, W., Cai, X., and Song, Y.: Determining the fluctuation of PM2.5 mass concentration and its applicability to Monin-Obukhov similarity, Science of the Total Environment, 710, 10.1016/j.scitotenv.2019.136398, 2020.
[14] Ripamonti, G., Jarvi, L., Molgaard, B., Hussein, T., Nordbo, A., and Hameri, K.: The effect of local sources on aerosol particle number size distribution, concentrations and fluxes in Helsinki, Finland, Tellus B., 65, 10.3402/tellusb.v65i0.19786, 2013.
[15] Rosenfeld, D., Andreae, M. O., Asmi, A., Chin, M., de Leeuw, G., Donovan, D. P., Kahn, R., Kinne, S., Kivekas, N., Kulmala, M., Lau, W., Schmidt, K. S., Suni, T., Wagner, T., Wild, M., and

https://doi.org/10.5194/egusphere-2023-2677
Preprint. Discussion started: 16 November 2023

Quaas, J.: Global observations of aerosol-cloud-precipitation-climate interactions, Reviews of Geophysics, 52, 750-808, 10.1002/2013rg000441, 2014.

[16] van de Hulst, H. C.: Light Scattering by Small Particles, John Wiley & Sons, Inc., New York, 1957.

[17] Vogt, M., Nilsson, E. D., Ahlm, L., Martensson, E. M., and Johansson, C.: Seasonal and diurnal cycles of 0.25–2.5 μ m aerosol fluxes over urban Stockholm, Sweden, Tellus B., 63, 935-951, 10.1111/j.1600-0889.2011.00551.x, 2011.

[18] Wang, T. I., Ochs, G. R., and Clifford, S. F.: Saturation-resistant optical scintillometer to measure Cn2, J. Opt. Soc. Am, 68, 334-338, 1978.

[19] Webb, E. K., Pearman, G. I., and Leuning, R.: Correction of flux measurements for density effects due to heat and water-vapor transfer, Quarterly Journal of the Royal Meteorological Society, 106, 85-100, 10.1002/qj.49710644707, 1980.

[20] Wilczak, J. M., Oncley, S. P., and Stage, S. A.: Sonic anemometer tilt correction algorithms, Boundary-Layer Meteorology, 99, 127-150, 10.1023/a:1018966204465, 2001.

[21] Wyngaard, J. C., Izumi, Y., and Collins, S. A.: Behavior of refractive-index-structure parameter near ground, Journal of the Optical Society of America, 61, 1646-&, 10.1364/josa.61.001646, 1971.

[22] Yuan, R., Luo, T., Sun, J., Zeng, Z., Ge, C., and Fu, Y.: A new method for measuring the imaginary part of the atmospheric refractive index structure parameter in the urban surface layer, Atmospheric Chemistry and Physics, 15, 2521-2531, 10.5194/acp-15-2521-2015, 2015.

[23] Yuan, R., Luo, T., Sun, J., Liu, H., Fu, Y., and Wang, Z.: A new method for estimating aerosol mass flux in the urban surface layer by LAS, Atmos. Meas. Tech. Discuss., doi:10.5194/amt-2015-301, 2016.

[24] Yuan, R., Zhang, X., Liu, H., Gui, Y., Shao, B., Tao, X., Wang, Y., Zhong, J., Li, Y., and Gao, Z.: Aerosol vertical mass flux measurements during heavy aerosol pollution episodes at a rural site and an urban site in the Beijing area of the North China Plain, Atmospheric Chemistry and Physics, 19, 12857-12874, 10.5194/acp-19-12857-2019, 2019.

[25] Yuan, R., Shi, C., Liu, H., Wang, Y., Qiao, B., and Wang, Z.: A method for estimating the ratio of aerosol mass concentration to the imaginary part of the atmospheric complex refractive index and its application, Atmospheric Research, 264, 10.1016/j.atmosres.2021.105848, 2021.

[26] Yuan, R. M., Kang, M., Park, S. B., Hong, J., Lee, D., and Kim, J.: Expansion of the planar-fit method to estimate flux over complex terrain, Meteorology and Atmospheric Physics, 110, 123-133, 10.1007/s00703-010-0113-9, 2011.

[27] Zhang, H., and Zhang, H.: Comparison of Turbulent Sensible Heat Flux Determined by Large-aperture Scintillometer and Eddy Covariance over Urban and Suburban Areas, Boundary-Layer Meteorology, 154, 119-136, 10.1007/s10546-014-9965-8, 2015.

[28] Zhao, J., Olivas, P. C., Kunwor, S., Malone, S. L., Staudhammer, C. L., Starr, G., and Oberbauer, S. F.: Comparison of sensible heat flux measured by large aperture scintillometer and eddy covariance in a seasonally-inundated wetland, Agricultural and Forest Meteorology, 259, 345-354, 10.1016/j.agrformet.2018.05.026, 2018.

https://doi.org/10.5194/egusphere-2023-2677
Preprint. Discussion started: 16 November 2023

Figures

Figure 1. Photographs of the measurement site. (a) Map of Hefei City and (b) expanded view of the measurement site on the USTC campus, which is marked as the red rectangle in (a). Points T and R in (b) show the locations of the transmitter and receiver, respectively. Point P in (b) marks the meteorological tower position. There are four heavy traffic roads surrounding the measurement site. Figures 1a and b @ Baidu are from website:

https://map.baidu.com/@13055953.105500832,3719556.851423825,15.3z/maptype%3DB_EARTH_MAP

https://doi.org/10.5194/egusphere-2023-2677
Preprint. Discussion started: 16 November 2023

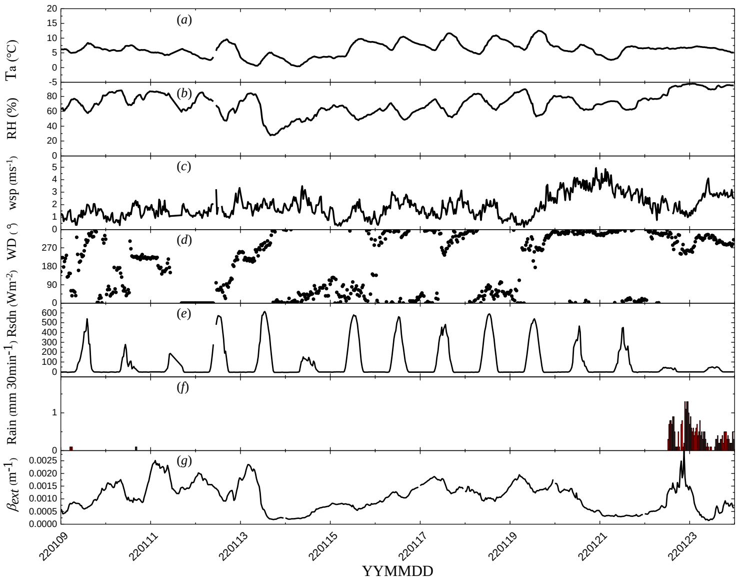

Figure 2. Temporal variations in the (a) air temperature (T), (b) relative humidity (RH), (c) wind speed (wsp), (d) wind direction (WD), (e) total radiation (Rsdn), (f) precipitation (Rain), and (g) extinction coefficient (β_{ext}). Details can be found in the text.

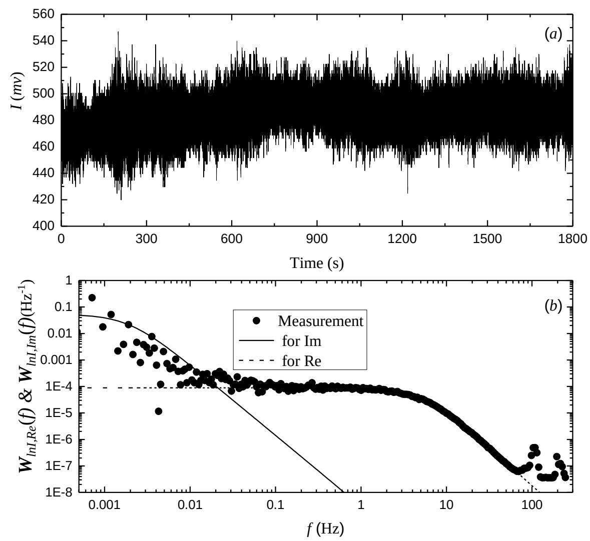

Figure 3 Temporal variations in the light intensity received by the LAS and (b) power spectral density of logarithm light intensity during 2022-01-16 13:00-13:30.

https://doi.org/10.5194/egusphere-2023-2677
Preprint. Discussion started: 16 November 2023

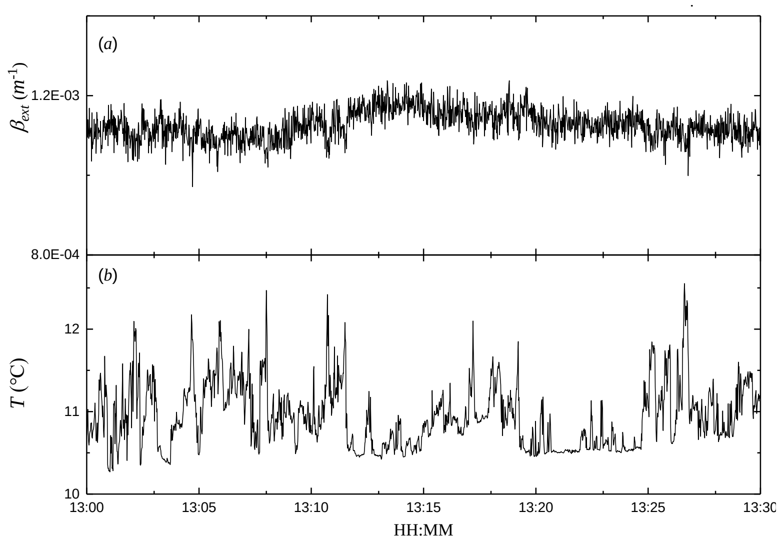

Figure 4 Temporal variations in (a) extinction coefficient and (b) air temperature during 2022-01-16 13:00-13:30.

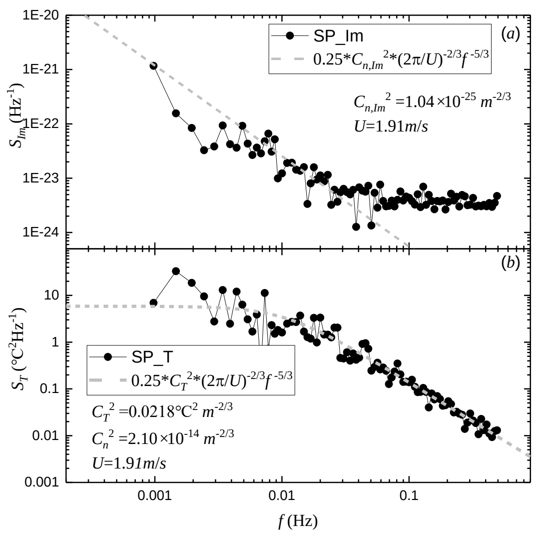

Figure 5. Power spectral density of (a) extinction coefficient and (b) air temperature during 2022-01-16 13:00-13:30.

https://doi.org/10.5194/egusphere-2023-2677
Preprint. Discussion started: 16 November 2023

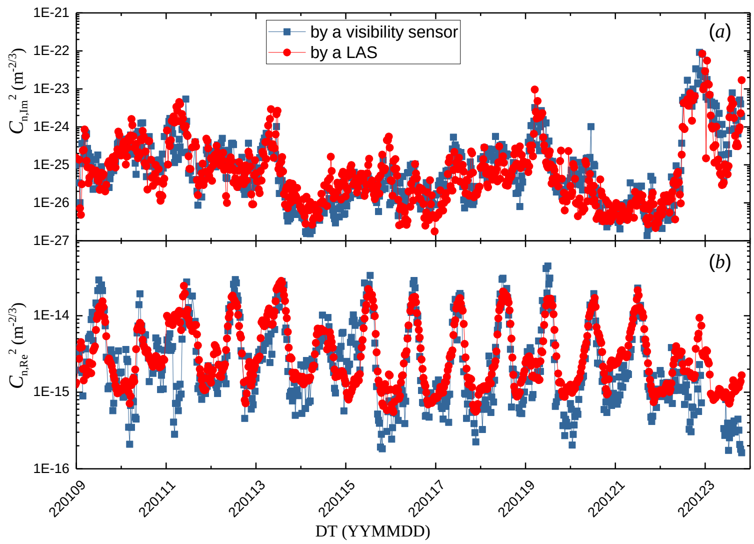

Figure 6. Temporal variations in (a) the imaginary part and (b) real part of the AERISP during 09-23 Jan. 2022.

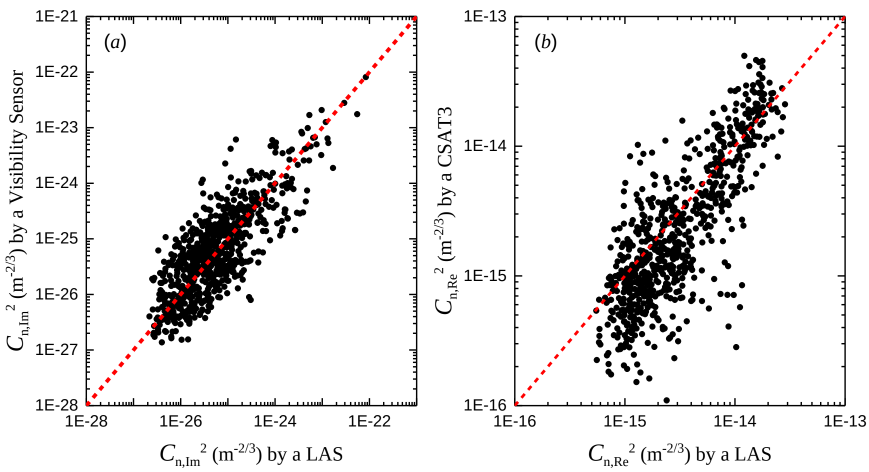

Figure 7. Comparison of (a) the imaginary part and (b) real part of the AERISP during 09-23 Jan. 2022.

https://doi.org/10.5194/egusphere-2023-2677
Preprint. Discussion started: 16 November 2023

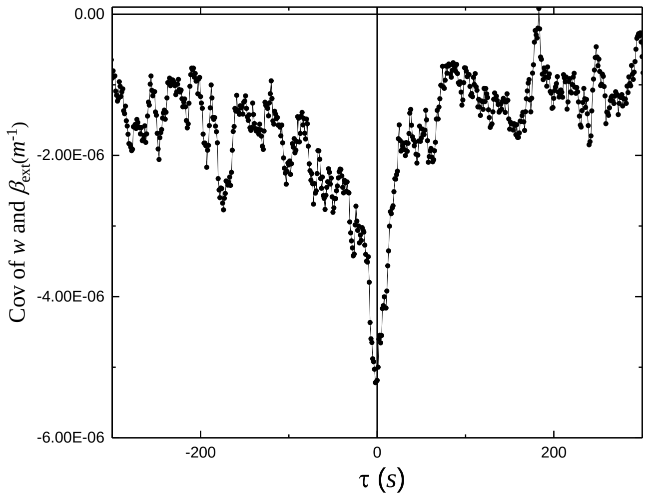

Figure 8. (a) Delay covariance between the extinction coefficient and vertical velocity during 2022-01-16 13:00-13:30.

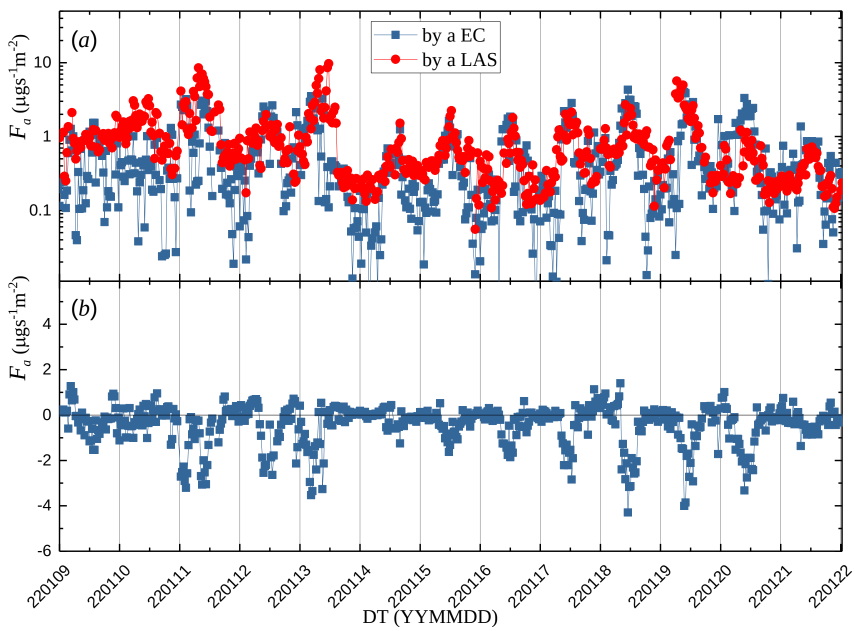

Figure 9. Temporal variations in (a) absolute value of aerosol flux based on the AERISP and EC methods and (b) the imaginary part and (b) aerosol flux based on the EC methods during 09-21 Jan. 2022.